ELSEVIER

PII: S0032-3861(97)00328-5

Polymer Vol. 39 No. 4, pp. 811–819, 1998

0032-3861/97/$17.00+0.00

Simultaneous measurement of water and polymer concentration profiles during swelling of poly(ethylene oxide) using magnetic resonance imaging

Thomas M. Hyde and Lynn F. Gladden*
Department of Chemical Engineering, University of Cambridge, Pembroke Street, Cambridge CB2 3RA, UK
(Received 25 July 1996; revised 8 January 1997)

A one-dimensional, slice-selective magnetic resonance imaging (MRI) technique is used to image *in situ* the penetration of water into poly(ethylene oxide) (PEO). Spin–lattice relaxation time (T_1)-weighted imaging experiments provide simultaneous, quantitative measurements of polymer and water concentration profiles, penetrant front motion kinetics and swelling kinetics. The propagation of the penetrant front is observed to be a diffusion-controlled process, with no volume change on mixing during swelling. Excellent agreement is observed when comparing the polymer concentration profiles obtained from the T_1 analysis with those measured by ^1H imaging of PEO during penetration by D_2O, under which conditions only the polymer response is imaged. © 1997 Elsevier Science Ltd.

(Keywords: magnetic resonance imaging; poly(ethylene oxide); two-component n.m.r. relaxometry)

INTRODUCTION

The main objective of this work was to develop an experimental technique that allows the determination of quantitative water and polymer concentration profiles, and hence swelling dynamics in hydrogel systems *in situ*. Hydrogels are of interest in the context of 'smart' materials (physicochemically sensitive gels)[1] and in polymeric controlled drug delivery systems[2,3]. The hydrogel chosen for study in this work is poly(ethylene oxide) PEO, which swells extensively in water due to strong hydrogen bonding between the water and the polymer[4] and can be considered as a model hydrogel system. PEO-based polymers have found widespread applications as biomaterials because PEO is particularly biocompatible and is mechanically tough due to its partially crystalline structure[5]. These polymers have been used for the engineering of liver, nerve, skin and breast tissue; the encapsulation of secretory cells in an implantable device; and the formation of barriers between tissues to prevent postsurgical adhesions[6]. They are also of interest as fabric coatings[7]. A PEO-based polymer has also been used for the controlled delivery of prostaglandin E_2, used for the ripening of the cervix in women at full term in labour[8]. The inertness of PEO to biological macromolecules also makes it an ideal material for incorporating cells into prosthetic devices[6]. The development of theoretical models for liquid transport and swelling within hydrogel systems has been limited through the lack of experimental data for the time-dependent spatial distribution of the liquid in the polymer, and has largely relied on gravimetric measurements to follow swelling kinetics. Techniques that have been previously employed include: X-ray microradiography[9]; optical microscopy[10]; electron spin resonance[11]; Rutherford back-scattering spectrometry[12]; and Fourier transform infrared attenuated total reflection spectroscopy[13]. Most of these techniques are invasive and the sample preparation processes required often result in the destruction of the sample.

In recent years, magnetic resonance imaging (MRI) has been used to study the transport of liquids in several polymer systems, and its potential as a non-invasive technique for obtaining spatial information has been demonstrated. An excellent review of the use of nuclear magnetic resonance (n.m.r.) and MRI in polymer science is given by Blümich and Blümer[14]. The technique has been applied to glassy polymers such as poly(methyl methacrylate) (PMMA)[15–18] and polystyrene (PS)[19,20]; and to rubbery polymers such as nylon[21–23] and vulcanised rubber[24–26]. More recently, MRI has been applied to study the swelling of ultrahigh molecular mass poly(ethylene) by the solvent decalin [27], and to study hydrophilic polymers for controlled drug release applications[28–30].

In general, in the imaging of liquid transport in polymers, the n.m.r. relaxation properties of the polymer are such that no signal is received from it. This has been seen as an advantage of MRI since it allows the liquid in the polymer to be selectively imaged. For example, under such conditions a detailed analysis of the dynamics of the penetrant within the polymer can be performed[22]. However, in highly swelling systems in particular, the use of MRI is complicated when a significant signal is received from the polymer as well as the liquid and, further, when the signals from the two overlap such that chemical shift techniques (traditionally used to resolve different chemical species) cannot be employed. Recently, Tabak and Corti[19] used MRI to study the polymer chain mobility in PMMA and PS by using deuterated liquids

* To whom correspondence should be addressed

(from which no signal is received in an n.m.r. probe tuned to the proton (^{1}H) resonance only). Halse *et al.*[31] have imaged both the liquid and polymer in a system consisting of natural rubber in decane. The polymer chains were highly mobile so that significant signal was obtained from both the polymer and the liquid. The liquid and polymer were imaged separately by exploiting the differences in the ^{1}H n.m.r. relaxation times of the two components.

In this work we extend the approach of Halse *et al.*[31] and present a new one-dimensional technique for the simultaneous measurement of the polymer and water distribution in a high-swelling polymer *in situ*, from a single experiment. This is possible because the polymer and water contributions to the observed ^{1}H signal can be isolated from the total ^{1}H signal by means of their respective spin–lattice relaxation times. In this study, the sample is allowed to swell one-dimensionally along the length of a glass tube. This experimental design has been selected for two reasons. First, the uptake kinetics are not distorted by the effects of anisotropic swelling[32]. Second, one-dimensional MRI can be used, which greatly reduces the acquisition time relative to two-dimensional imaging. This is of particular importance in hydrogel studies where the liquid penetration occurs over timescales of minutes.

MAGNETIC RESONANCE IMAGING

Nuclear magnetic resonance

When nuclei that have a non-zero nuclear spin quantum number, such as ^{1}H, are placed in an external magnetic field, $\mathbf{B}_0$, the individual components of the magnetic moment of each spin (having a state of $+\frac{1}{2}$ or $-\frac{1}{2}$) can be considered to be a vector which is aligned parallel or antiparallel to the magnetic field. The net difference between the populations of the two spin states gives rise to an overall magnetisation, which is treated as a vector aligned at equilibrium with the $\mathbf{B}_0$ field, taken as the z-direction by convention. In n.m.r. experiments the magnetisation vector, $\mathbf{M}$, is manipulated by a second magnetic field, $\mathbf{B}_1$, which is supplied through the pulsed application of radio frequency (r.f.) energy and acts at right-angles to $\mathbf{B}_0$. The r.f. pulses induce resonant transitions between the two different spin states, thereby rotating $\mathbf{M}$ into the x–y plane relative to a frame of reference rotating at the Larmor frequency. The Larmor frequency, ω_0, is the resonant frequency of the spin system in the presence of $\mathbf{B}_0$, and is defined by:

$$\omega_0 = \gamma B_0 \tag{1}$$

where γ is the magnetogyric ratio of the nucleus under study.

The magnitude of $\mathbf{M}$ at thermal equilibrium, M_0, is directly proportional to the number of resonant spins in the system under study; hence n.m.r. is an inherently quantitative technique. A full description of the manipulation of the magnetisation by r.f. pulses is given elsewhere (for example, see Fukushima and Roeder[33]).

Spin–lattice and spin–spin relaxation

As described above, the magnetisation of the spin system is perturbed from equilibrium by the application of r.f. energy. There are two relaxation processes involved in the return of the magnetisation of the spin system to equilibrium, corresponding to energy transfer between the excited spins and the surrounding lattice, and energy transfer within the spin system itself. These processes are referred to as spin–lattice and spin–spin relaxation, respectively. Spin–lattice relaxation is responsible for the return of the longitudinal component of magnetisation (relative to the direction of the magnetic field) to its equilibrium value, and is described by:

$$\frac{dM_z}{dt} = -\frac{(M_z - M_0)}{T_1} \tag{2}$$

where T_1 is the time constant for the relaxation process.

The relaxation of the transverse component of the magnetisation — spin–spin relaxation — is the process by which the nuclear spins come to equilibrium with themselves. Spin–spin relaxation controls the rate of decay of phase coherence amongst nuclear spins in the x–y plane, and is characterised by a time constant T_2, such that:

$$\frac{dM_{xy}}{dt} = -\frac{M_{xy}}{T_2}. \tag{3}$$

The T_1 and T_2 properties of a liquid in a solid are descriptive of energy exchange and are dependent on the degree of interaction between the spins and the surrounding thermal reservoir or lattice. Because of this, the measurement of T_1 and T_2 allows the study of the physical and chemical properties of materials. Weisenberger and Koenig[17] have studied the spatial dependence of the T_1 and T_2 values of methanol in PMMA and found them to be highly dependent on the polymer environment. They related the relaxation behaviour to both short- and long-range liquid–polymer interactions, such as the mobility of polymer segments relative to adjacent liquid molecules. More recently, the present authors have investigated the change in T_1 and T_2 of liquids in polymers, both for the quantitative use of MRI in 'high-contrast' systems[27] and as a probe of polymer structure and drug-phase distribution[30]. Tabak and Corti[19] have directly measured the T_1 relaxation properties of the polymer in the PMMA and PS systems they studied. They observed a gradient in T_1 through the homogeneously swollen region of the sample, which indicated a change in polymer chain mobility. Halse *et al.*[31] observed the same behaviour for the T_2 of natural rubber when swollen in decane. There have also been many solid-state n.m.r. studies carried out relating the n.m.r. relaxation properties of polymers to polymer motion and motional transitions; this area of research has been reviewed by Cheng and Early[34]. The focus of this work is to probe directly the T_1 properties of both the penetrating liquid and the polymer.

Spin–echo imaging

MRI utilises a magnetic field gradient, $\mathbf{G}$, which is applied in addition to the uniform field, $\mathbf{B}_0$. The resultant resonant frequency of the nuclear spins is dependent on the spatial position of the molecules within the sample (as denoted by the vector $\mathbf{r}$), and is given by:

$$\omega(\mathbf{r}) = \gamma B_0 + \gamma \mathbf{G}\cdot\mathbf{r}. \tag{4}$$

Spin–echo imaging[35] is a well established MRI technique that exploits this principle, and several of its forms are described by Callaghan[36]. The pulse sequence used in this work is based on the standard spin–echo technique and is shown in *Figure 1*. The r.f. pulse sequence is very similar to the standard two-dimensional imaging technique most often used except that there is no phase encoding, and there is a saturation–recovery preconditioning step to produce T_1 contrast in the system[26]. Application of this particular pulse sequence acquires data in the form of a

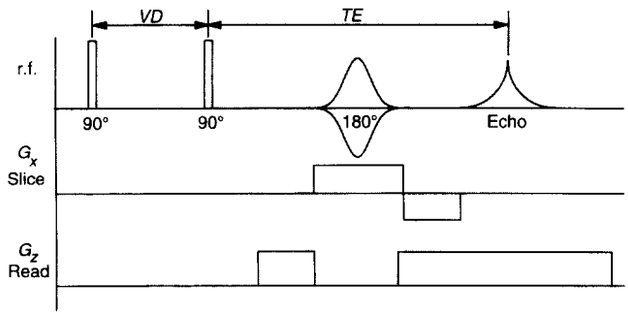

Figure 1 Imaging pulse sequence used to obtain T_1-weighted profiles across a selectively excited slice. The sequence consists of a standard spin–echo sequence with the phase encoding switched off and employs a selective 'soft' 180° r.f. pulse. The spin system is preconditioned with a hard 90° pulse separated from the imaging sequence by a variable delay, *VD*, to produce T_1 contrast

one-dimensional slice image through the polymer sample. A 90° r.f. pulse rotates the magnetisation of the system into the x–y plane. A variable delay time, *VD*, is allowed for relaxation of the longitudinal component of the magnetisation. If the length of *VD* is such that the magnetisation does not recover to equilibrium, then the resulting one-dimensional signal intensity profile is referred to as 'T_1-weighted', as the signal will be attenuated by T_1 contrast. The recovered magnetisation component is again rotated into the x–y plane by a second 90° pulse, after which the spins begin to dephase. Following this the read gradient is applied. Next, an image slice through the sample is selectively excited using a 'soft' 180° pulse in conjunction with a slice-selective gradient[37]. Only the magnetisation of spins whose resonant frequencies fall within the bandwidth of the soft pulse will be rotated by 180°, and hence be imaged. The inversion of the magnetisation components by the 180° pulse causes the spins to rephase, which results in the formation of an 'echo'. The time from when the second 90° pulse is applied to when the echo forms is referred to as the 'echo time', *TE*, and is equal to twice the time between the 90° and 180° pulses. A refocussing gradient is applied after the slice-selective gradient to reverse dephasing effects. The read gradient is again applied and the echo is recorded in the time domain. Repeated scans are accumulated to improve the signal-to-noise ratio, and a recycle delay time must be allowed between scans to allow the magnetisation to recover to equilibrium. On completion of data acquisition, the time-domain signal is Fourier transformed to yield an image, or in this case a profile, in the frequency domain.

Measuring spatially resolved T_1 values

As discussed earlier, the study of the T_1 properties of a liquid–polymer system can be used as a physicochemical probe of both the liquid and the polymer, and their interactions. The spatially resolved T_1 values can be obtained for a single species by measuring a series of T_1-weighted one-dimensional profiles (i.e. at a range of values for *VD* in the pulse sequence described in *Figure 1*) and, for each image pixel, fitting the intensity values, I_i, as a function of *VD* to:

$$I_i = I_{0,i}\left[1 - \exp\left(-\frac{VD}{T_{1,i}}\right)\right] \quad (5a)$$

$I_{0,i}$ represents the signal intensity that would be obtained in the absence of T_1-contrast, while $T_{1,i}$ is the spin–lattice relaxation time for the single species in the ith voxel element. If the n.m.r. signal is received from two species — the polymer chains *and* the liquid molecules, for example — then equation (5a) can be written in a two-component form:

$$I_i = I_{0,1,i}\left[1 - \exp\left(-\frac{VD}{T_{1,1,i}}\right)\right] + I_{0,2,i}\left[1 - \exp\left(-\frac{VD}{T_{1,2,i}}\right)\right] \quad (5b)$$

$T_{1,1,i}$ and $T_{1,2,i}$ are the T_1 relaxation times for components 1 and 2, respectively, and the unattenuated intensities, $I_{0,1,i}$ and $I_{0,2,i}$, are measures of the relative amounts of species 1 and 2 that are present in the voxel.

EXPERIMENTAL

Sample preparation

Poly(ethylene oxide) ($M_w = 4 \times 10^6$ g mol^{-1}) was crosslinked with 1.0 wt% lupersol (2,5 dimethyl-2,5 di(*t*-butylperoxy)hexyne 3)) in a circular mould at 180°C, for 10 min, under pressure. The resulting disc, which was approximately 3 mm thick, was removed from the mould and annealed at 110°C for 45 min prior to slow cooling to room temperature. To manufacture a sample for the constrained swelling experiment, a portion of the slab was cut to a cylindrical geometry such that it fitted inside a glass tube with an inner diameter of 2.74 mm and a length of 50 mm. The typical mass of the cut polymer portion was 0.019 g. The polymer was placed in the glass tube which was inserted into a brass tube which had screws at each end. The screws supported Teflon blocks which pressed against the exposed faces of the polymer, thereby producing a polymer sample with flat end-surfaces in the middle of the tube. The apparatus containing the polymer sample was placed in an oven at 110°C for 10 min, without pressure applied, to relieve any stresses in the sample. The screws were then tightened as far as possible and the sample left for a further 10 min. The apparatus was removed from the oven and cooled to room temperature with continuous pressure applied to counter the thermal contraction of the polymer. The resulting sample was 2.7 mm in diameter and approximately 3 mm in length.

MRI

The imaging experiments were conducted on a Bruker DMX 200 (4.7 T) spectrometer equipped with microimaging probehead tuned to 200.13 MHz for the proton (^{1}H) resonance. The probe insert consisted of a vertical saddle coil with a diameter of 5 mm. The glass tube containing the polymer sample was removed from the sample preparation apparatus and placed in the microimaging probe. Either deionised water (H_2O) or deuterated water (D_2O) was placed at the ends of the sample before it was placed in the n.m.r. microimaging probe. Using the imaging technique described earlier, a 0.5 mm slice was excited along the length of the sample tube, which was oriented vertically in the insert.

An automation program was employed that at prescribed intervals (typically 4, 15, or 30 min) acquired eight signal intensity profiles using a range of *VD* values. Each 512-pixel profile was formed by coadding the signal from two scans. At each time point in the experiment the eight T_1-weighted profiles were stored in a 512 × 8 array. These arrays were in turn stacked in a three-dimensional block. The read and slice gradients were 15.66 and 39.46 G cm^{-1}, respectively, while the field-of-view was 15 mm, giving an in-plane

resolution of 29.3 μm. The spectral width was 100 kHz and an echo time of 5.65 ms was used. The n.m.r. spectrum for H_2O-swollen PEO consisted of a single sharp peak, indicating that the water and polymer proton signals fully overlapped, with a line-width of only 100 Hz. Buszko and Maciel[38] observed a very similar spectrum for unswollen PEO. The line-width for a liquid in a solid is often several kHz due to T_2 broadening, and this will lead to a loss of resolution in the images if the line-width exceeds the band-width of a single pixel. The narrow line-width observed in this work caused no such loss of resolution as it was much smaller than the pixel band-width.

Several samples were imaged for reproducibility, and a calibration sample of pure water (containing a known number of ^1H spins) was imaged at various intervals so that quantitative concentration profiles could be obtained. The swelling experiments were conducted at room temperature (21.0 ± 0.5°C) *in situ*. Swelling was monitored, *ex situ*, by measuring the length of the sample with vernier callipers, and the final degree of swelling was determined gravimetrically.

RESULTS AND DISCUSSION

The results obtained in this study are reported in three sections. First, a brief investigation of the polymer profiles during swelling by D_2O is described in which the general features of the polymer response during penetration and swelling are observed directly without any need for post-acquisition data analysis. Second, the simultaneous determination of water and polymer concentration profiles is described, and the validation of this approach by comparison of the polymer profiles so obtained with those measured following D_2O penetration of PEO is discussed. It is also demonstrated that by employing an experimental configuration in which the polymer is penetrated by H_2O and D_2O from opposite ends, ^1H imaging allows the measurement of the H_2O profile through the gel even after the penetrant fronts have met. A brief discussion of the trends in the spin–lattice relaxation characteristics of the polymer and water protons during swelling is also presented. Finally, the polymer and water concentration profile data are used to study the kinetics of penetrant front motion and the swelling kinetics of the water–PEO system.

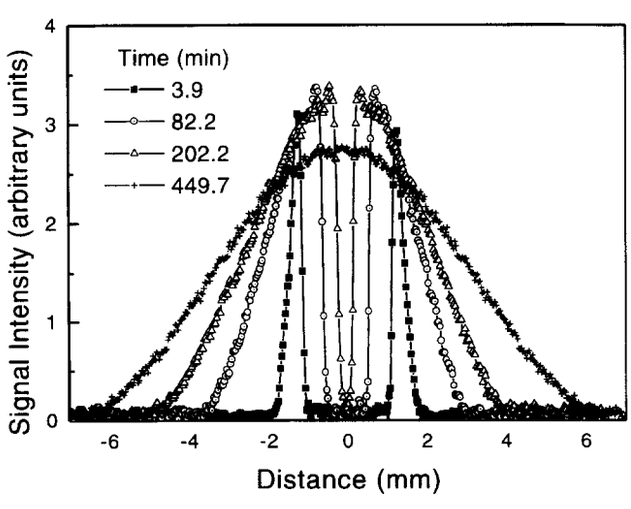

Figure 2 Intensity profiles of the polymer distribution in the swollen polymer — the deuterated water diffuses from both ends. The two sharp penetrant fronts are visible and move towards each other

Polymer response during swelling

Separate ^1H MRI studies of polymer loaded with H_2O, and with D_2O, showed that significant signal was generated by the polymer in the swollen or 'gelled' material. It was therefore possible to selectively image the ^1H response of the polymer in the gel by using D_2O as the penetrant. *Figure 2* shows a series of one-dimensional selective slice profiles for a sample undergoing D_2O penetration from both ends. These data were obtained using a recycle delay and *VD* of 5 s. Characterisation of the T_1 of the polymer showed that it was typically 0.4 s (this is examined in more detail in the following section). The T_2 of the polymer was typically 50–100 ms which, relative to the echo time (5.65 ms), meant there was minimal T_2 contrast. The magnitude of T_1 relative to the recycle delay allowed contrast-free profiles to be obtained without having to conduct a full T_1-weighted experiment. Each profile took 10 s to acquire. Several features are apparent from *Figure 2*. First, there are two sharp boundaries between the penetrated and unpenetrated polymer that move towards each other with time; behind these penetrant 'fronts' the sample swells, as indicated by the continually broadening profile. Second, the polymer signal intensity at the fronts increases with time, indicating an increase in concentration of polymer at the penetrant–polymer interface as penetration proceeds. Third, the penetrant fronts meet after approximately 3.5 h and the polymer continues to flow away from the interface, giving a profile that is rounded in the middle. The imaging of the polymer allows us to study what is essentially the diffusion of the polymer through the water–polymer mixture. The sample swells from an initial length of 2.7 mm to 12 mm in 7.5 h, and continues to swell until equilibrium is reached.

Simultaneous imaging of water and polymer during swelling

In the experiment described in this section, the T_1-contrast technique is used to simultaneously image both the water and polymer within the swollen polymer. This approach is validated by comparing the polymer profile obtained with that measured directly for D_2O penetration occurring within the same system.

A constrained swelling experiment was conducted on a sample of PEO with H_2O placed at the top and D_2O at the bottom. In this case the full T_1-weighted experiment was conducted with variable delays (*VD* values) of 3.0, 2.0, 1.0, 0.5, 0.3, 0.2 and 0.1 s, and a recycle delay of 5 s. The acquisition time for the series of profiles at each time point was 84 s. The T_1-weighted profiles were fitted to equation (5b) using a chi-squared minimisation routine to obtain intensity profiles for the two components, namely the water and polymer molecules, in the H_2O-impregnated polymer. The profile recorded for the longest variable delay was used to obtain the distribution of polymer in the D_2O-impregnated polymer.

Figure 3 shows typical profiles obtained for a sample after 36 min of diffusion and swelling. The H_2O profile (at left) shows that there is a concentration gradient of water in the gelled region of the polymer. The polymer profile obtained by two-component T_1 fitting (at left) is in very close agreement with the profile obtained by directly recording the polymer signal from the end of the sample that was impregnated with D_2O (at right). The data for the water and polymer profiles at the H_2O-impregnated end of the sample show more scatter than those for the directly measured polymer profile. A possible reason for this, in addition to any error associated with the multicomponent

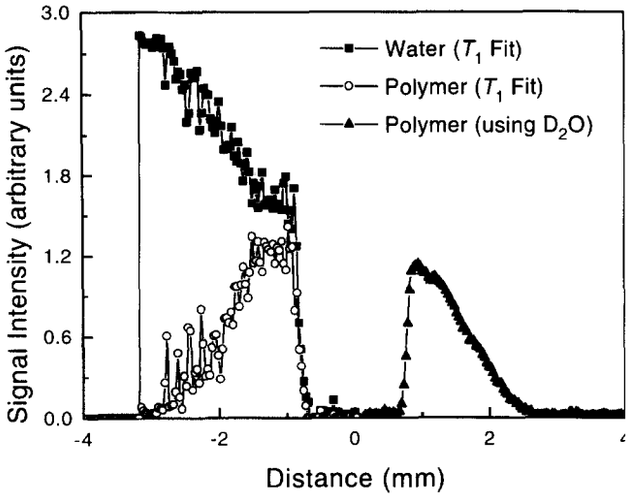

Figure 3 Profiles of the water and polymer in a sample undergoing diffusion by H_2O from the top and by D_2O from the bottom, after 36 min. The profiles in the H_2O-loaded end were obtained by fitting equation (5b) to T_1-weighted profiles

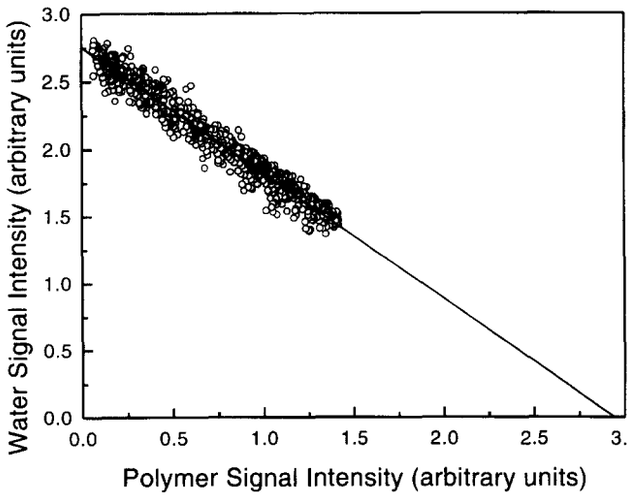

Figure 4 Water signal intensity *versus* polymer signal intensity in H_2O-penetrated PEO. The line shown is that of a linear least squares fit to the data, as discussed in the text

fitting technique, is that the profiles obtained by T_1-fitting are very susceptible to small changes in the n.m.r. relaxation properties of the polymer gel. For example, it was observed that very small air bubbles formed in the gel during penetration. Scatter in the calculated profiles might be produced by such air bubbles since they would be expected to cause local variations in the spin–lattice relaxation time associated with the water molecules; this scatter would also be seen in the polymer profile data since the latter are calculated from the same image intensity profile. The observation that no such variation in the T_1-weighted profiles obtained from D_2O-loaded polymer was observed is taken as evidence that it is the water T_1 that is almost exclusively sensitive to the presence of the air bubbles. *Figure 3* clearly illustrates that the multicomponent T_1-fitting technique, combined with one-dimensional selective-slice imaging, can be used to resolve the polymer and water distribution in a highly swelling hydrogel *in situ*.

Quantitative water and polymer concentration profiles were obtained by calibrating the water signal obtained from the intensity profile data against the water signal from a reference sample. Once the water concentration within each pixel is known, the polymer concentration profiles can also be obtained. An important observation in the context of this analysis is that the data obtained in this study are consistent with there being no change in volume on swelling; that is, the volume of the gelled polymer is equal to the sum of the volumes of the water and polymer phases. The intensities corresponding to water and polymer at each pixel, for several time points in the uptake, for the H_2O-impregnated end of the sample, are plotted in *Figure 4*. The line shown through the data was found by a linear least-squares fit and has a slope of -0.936 ± 0.007, an intercept of 2.75 ± 0.08, and a regression coefficient of 0.978. The fact that data do not exist below water intensities of approximately 1.5 is indicative of the fact that the penetrant front is very sharp, with the water concentration almost discontinuous at the interface between the swollen and unswollen polymer. The analysis now proceeds as follows. If the contrast-free signal intensity of water, I_w, is known for a given pixel (for example, if normal water has been used and I_w determined using two-component T_1 fitting) the volume fraction of water, ϕ_w, can be expressed by:

$$\phi_w = I_w / I_{ref}, \tag{6a}$$

where I_{ref} is the signal intensity of a reference sample of pure water. Further, following from the correlation observed between the polymer and water signal intensities (*Figure 4*), if the intensity of the polymer signal is known (either by T_1 fitting of the signal obtained using H_2O, or by direct measurement using D_2O), we can write, for the volume fraction of polymer, ϕ_p:

$$\phi_p = 0.936 \frac{I_p}{I_{ref}}, \tag{6b}$$

where I_p is the contrast-free signal intensity of the polymer for that voxel. The water volume fraction can, of course, also be calculated by difference from the polymer volume fraction if there is no change in volume on mixing:

$$\phi_w = 1 - \phi_p. \tag{6c}$$

The quantitative results obtained using equations (6a), (6b) and (6c) are compared in *Figure 5*(a) and (b), after penetration times of 32 and 112 min, respectively. Data from two samples are shown in each figure. Sample (1) has undergone D_2O penetration at both ends, while sample (2) has been penetrated by H_2O from the top and D_2O from the bottom. Let us consider first the profiles shown for sample (1): the solid line is the polymer profile, expressed in terms of volume fraction, as calculated using equation (6b), and the dotted line is the water concentration profile as calculated from the polymer profile using equation (6c). In calculating the water concentration profiles from the polymer profiles, the situation at the leading edge of the penetrant front is difficult to quantify. Here, the values of the water volume fraction have been assumed to be the same as those for the polymer volume fraction. Comparison of the water concentration profiles at the front, as obtained by two-component T_1 fitting, and by calculation from polymer profiles (as shown in *Figure 5*), show that the front is sharp and that the agreement between the two profiles at the sharp edge of the front is very good. For the case of sample (2), the squares and circles represent the water and polymer concentration data, respectively, as obtained using the two-component T_1 fitting technique for the H_2O-impregnated end of the

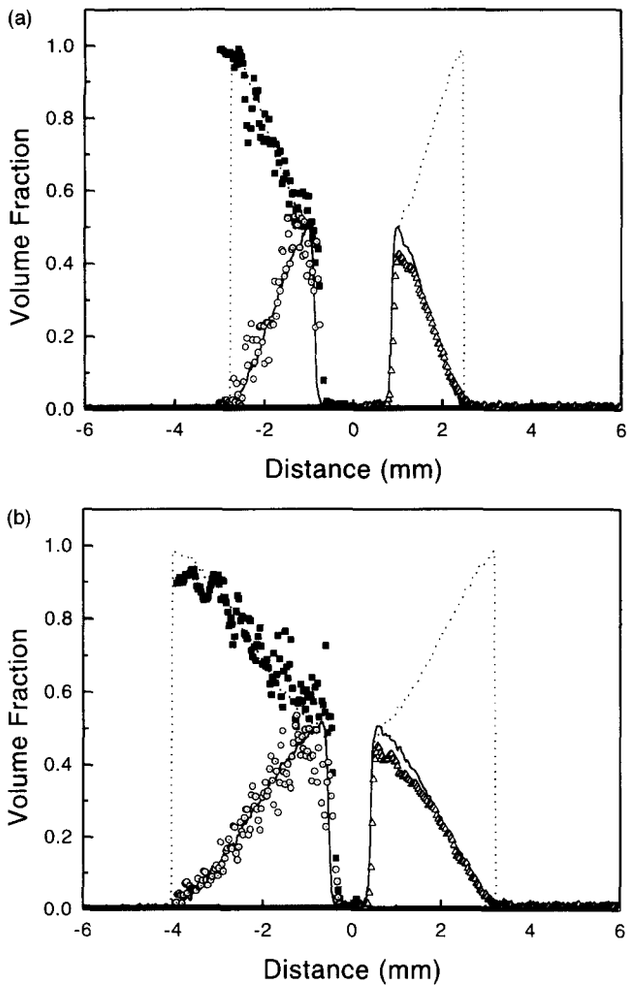

Figure 5 Water and polymer volume fraction profiles recorded for two samples. Sample (1) is being penetrated by D_2O from both ends; data are shown for polymer (—) and water (· · ·). Sample (2) is undergoing penetration by H_2O (from top) and D_2O (from bottom): (■) water (H_2O end); (○) polymer (H_2O end); and (△) polymer (D_2O end). The profiles are shown after diffusion and swelling for: (a) 32 min; (b) 112 min

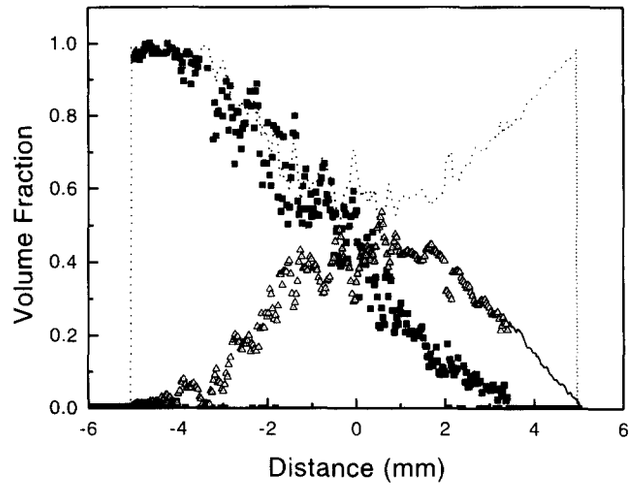

Figure 6 Water and polymer profiles in a sample undergoing penetration by both H_2O (from top) and D_2O (from bottom): (■) H_2O water concentration data; (· · ·) total water (D_2O and H_2O) concentration (from equation (6c)). The polymer profile is made up of data from T_1 fitting (△) and from direct measurement at the deuterated end of the sample (—)

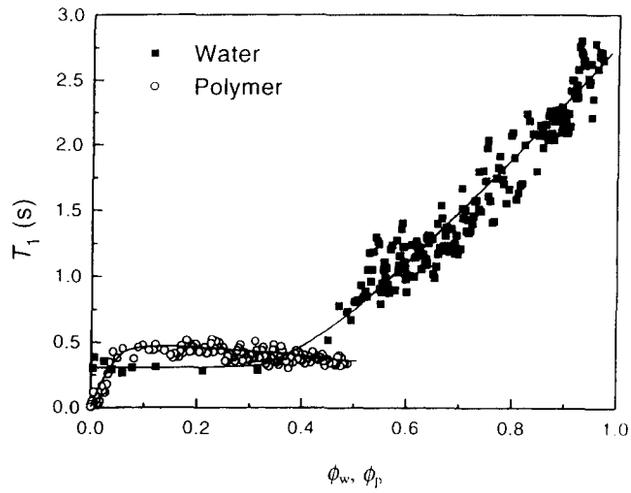

Figure 7 T_1 data for the water and polymer as a function of volume fraction, as obtained by the two-component technique (equation (5b)) for an H_2O-impregnated sample. Each data point represents the average of 9 values, and the data set was accumulated from the MRI measurements at 18 time points in the uptake process. Trends in the data are shown by polynomial fits

sample, combined with equations (6a and b), respectively. The triangles are the polymer concentration data obtained from the D_2O-impregnated end of the sample, using equation (6b).

A number of important conclusions can be drawn from the data shown in *Figure 5*. The agreement between the polymer concentration data obtained with deuterated penetrant for samples (1) and (2) is very good at both time points, again illustrating the reproducibility of the experiment. It is also seen that the front positions observed in both samples are in very close agreement. The agreement between the water concentration data calculated by difference for sample (1), and by two-component T_1 fitting for sample (2), is also very good. Hence, the assumption of no volume change on mixing is valid. The fact that the polymer profiles at the top end of the samples, measured directly for sample (1) and again by two-component T_1 fitting for sample (2), are within very close agreement confirms that the two-component T_1 fitting experiment does yield accurate concentration data.

A further feature of the experiment employing both H_2O and D_2O penetration is that it is possible to profile the motion of the H_2O through the gel even after the penetrant fronts have met. *Figure 6* shows the profiles obtained for a sample after undergoing H_2O and D_2O diffusion for 261 min. The H_2O has not yet penetrated through to the other side of the sample. The polymer profile is represented as a combination of the data found by two-component T_1 fitting (for the region containing D_2O, H_2O and PEO) and by direct measurement (for the region containing only D_2O and PEO). The square symbols in *Figure 6* represent the quantitative H_2O concentration profile. By comparing the total water concentration profile (the dotted line obtained from the polymer profile using equation (6c)) with the H_2O profile, it is seen that the H_2O profile is no longer sharp, and appears more like a classic Fickian concentration profile in the deuterated gel.

Figure 7 shows the spin–lattice relaxation time data obtained for an H_2O–PEO sample, using the two-component T_1 fitting technique. Each point represents

an average of nine values taken from the cumulative data from 18 profiles, which were measured at different time points in the uptake process. The consistency of the data shows that the T_1 relaxation times are dependent purely on concentration. For water the T_1 is relatively short and constant over the volume fraction 0–0.3, corresponding to the concentrations occurring at the penetrant front, indicating that the polymer–penetrant environment is homogeneous. The T_1 is shortest over this range, indicating efficient energy exchange between the water molecules and the polymer chains. At higher volume fractions the water T_1 increases rapidly and almost linearly across the range of concentrations found through the gelled region of the sample. This increase in the water T_1 with volume fraction in the gelled region of the polymer is as would be expected, due to the interactions between the water and polymer molecules becoming longer range. At high volume fractions the water in the gel begins to behave like free water, with the T_1 value approaching 3 s.

In the case of the polymer the T_1 values are similar to those for water over the volume fraction range 0.1–0.4. For volume fractions of approximately 0.5, corresponding to the polymer that is fully exposed to the water at the penetrant front, the polymer T_1 is approximately 0.4 s. As the polymer swells (such that the polymer volume fraction decreases) the T_1 increases slightly to approximately 0.5 s. The polymer volume fraction range 0–0.05 corresponds both to the polymer at the surface exposed to bulk water and to the polymer fraction that has partially gelled at the leading edge of the penetrant front. Over this range the T_1 of the polymer increases rapidly from 0 to 0.4 s. The observation that the T_1 of the polymer increases rapidly over the polymer volume fraction range 0–0.05 indicates that the spin environments in the partially hydrated gel at the penetrant front, and in the fully swollen gel at the edge of the sample, are very similar. The T_1 of the polymer in the gelled region of the sample is constant over much of the volume fraction range and appears to be dependent on whether or not the polymer has gelled, rather than on concentration. This suggests that the T_1 of the polymer molecules depends strongly on the mobility of the polymer chains, which is therefore largely unaffected by polymer concentration in the gel. The T_1 values obtained for the polymer for all fractions studied were identical, to within experimental error, regardless of whether the polymer was penetrated by H_2O or D_2O.

Penetrant front and swelling kinetics

The quantitative concentration profiles obtained allow the measurement of various aspects of the transport kinetics *in situ*. An important indicator of the rate-controlling process in the swelling of the polymer is the rate at which the polymer front moves[27,30,39]. As seen in the concentration profiles presented earlier, a sharp interface was observed between the swollen and the unpenetrated polymer. Typically, a sharp interface indicates a phase transition, such as the glass to rubber transition observed in the methanol–PMMA system[40], or a crystalline to amorphous transition as seen in water–PEO[5]. The propagation of the interface is dependent on the relative rates of polymer chain relaxation and diffusion. If the process is diffusion controlled, Fick's law holds[41] and the front will move proportional to $t^{1/2}$. *Figure 8* shows plots of the position, d, of the two penetrant fronts moving from the top and bottom of a sample, relative to the starting positions of the polymer sample surfaces, versus $t^{1/2}$. The data are linear with respect to $t^{1/2}$, indicating that the front propagation is a Fickian

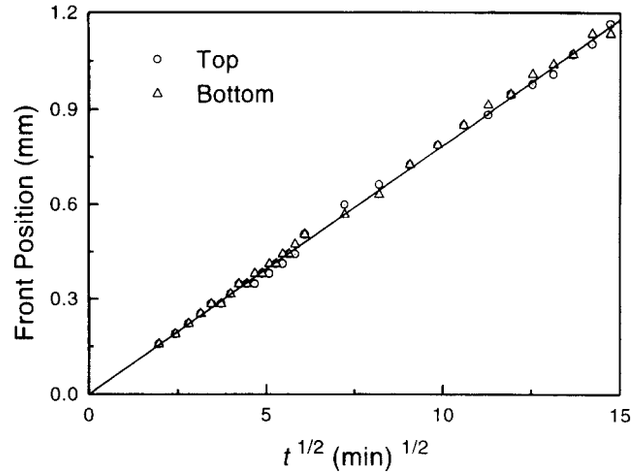

Figure 8 Plots of the positions of the penetrant fronts (relative to the initial positions of the sample surfaces) moving from the top and bottom of a sample, *versus* $t^{1/2}$. The linearity of the relationship, shown by the solid line, indicates that the front propagation is controlled by a diffusion process

Table 1 Front motion kinetics for water in PEO at 21°C. The rate constant, k_f, of the front propagation is given for water penetration from both the top and the bottom of the sample. The regression coefficients, R, of the fits to the two sets of data, from which the rate constants are obtained, are also given.

Penetrant front	k_f (m s$^{-1/2}$)	R
Top	$1.013 \pm 0.008 \times 10^{-5}$	0.9990
Bottom	$1.019 \pm 0.006 \times 10^{-5}$	0.9993

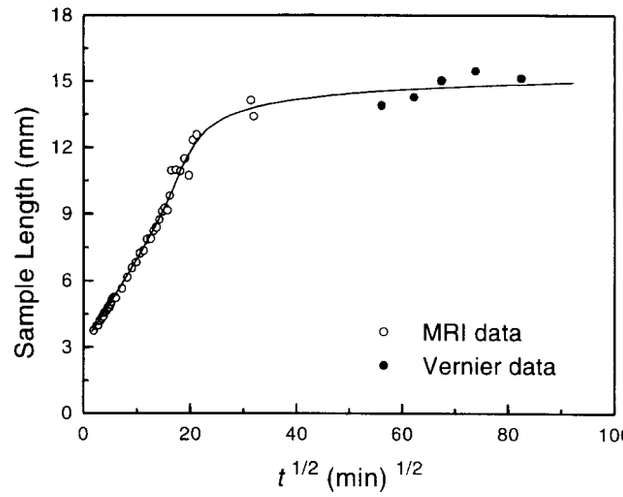

Figure 9 Sample length *versus* $t^{1/2}$. Data obtained, *in situ*, from MRI profiles are presented along with the measurements made *ex situ* with vernier callipers at long times. The trend in the data is shown by a polynomial fit

diffusion process. The agreement between the data sets is very good and the direction of the front motion, whether up or down, has no noticeable effect on the rate of motion. The line shown was fitted by linear least-squares regression. The front kinetics can be expressed by:

$$d = k_f t^{1/2} \tag{7}$$

where k_f is the rate constant characterising the penetration process. *Table 1* contains the values for k_f and tabulates the regression coefficients, R, for the fits to the data.

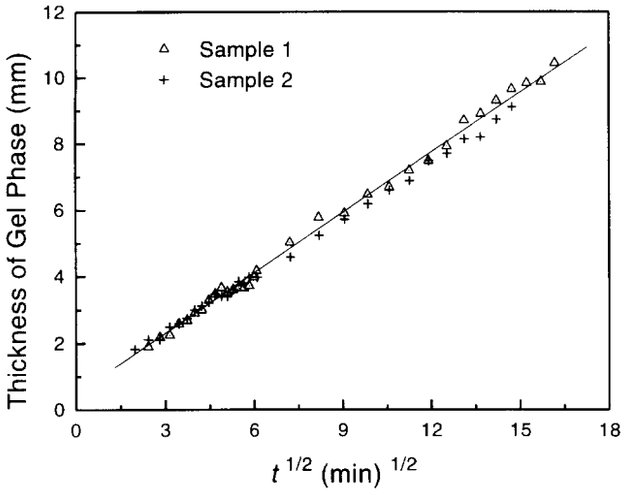

Figure 10 A comparison of the change in the total gel thickness, with $t^{1/2}$, for two samples. The line shown is that of a linear least-squares fit to the data

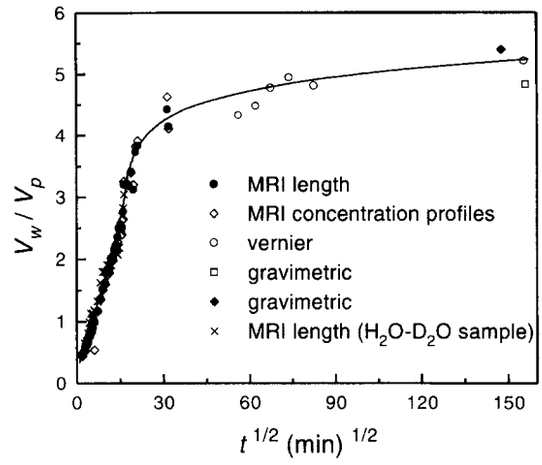

Figure 11 Volumetric swelling ratio *versus* $t^{1/2}$. The swelling kinetics were calculated from: MRI data (both length and concentration measurements); vernier calliper length measurements; and by gravimetric measurements. The trend in the data is shown by a polynomial fit

The one-dimensional profiles allow both the sample length and the thickness of the gelled portion of the sample to be measured. *Figure 9* shows the kinetic data for the change in length of a sample. The data obtained from MRI profiles are shown along with measurements made using vernier callipers at long times, when the sample had exceeded the field-of-view. The change in length shows a linear dependence with respect to $t^{1/2}$ up to about 4 h, the time when the penetrant fronts met, at which point there is a slight increase in slope. This effect was reproduced in all samples, and suggests that the inflection in the free swelling sorption curves of Graham and McNeill[32] may not have been purely due to anisotropic swelling effects.

Figure 10 shows the change in the combined thickness of the gel phases that exist in the polymer before the penetrant fronts meet. Data for two samples are presented to illustrate the reproducibility of the samples used in these experiments. The change in gel thickness with $t^{1/2}$ is linear, indicating that the increase in gel thickness is controlled by diffusion of water into the polymer; the same correlation with time is also observed for the thicknesses of the two individual gel-phase regions. In the concentration profiles a concentration gradient of water (and polymer) was found to exist in the fully penetrated gel. This accounts for the observed increase in sample length as a function of time after the penetrant fronts have met, as a driving force for diffusion still exists. The front motion, sample length and gel thickness kinetics for the H_2O-impregnated samples were very similar to those for the deuterated samples, suggesting that there was no significant difference in the interaction between H_2O and D_2O molecules with the polymer.

Several approaches were used to measure the swelling kinetics for water in PEO. The use of MRI allowed the swelling ratio to be determined from length measurements, and by integrating underneath the calculated concentration profiles. At long times, length measurements were made using vernier callipers. Finally, when it was deemed that samples had attained equilibrium, the final swelling ratio was obtained gravimetrically. When using length measurements, the volumetric swelling ratio (the ratio of volume of water to the volume of PEO), V_w/V_p, is calculated as:

$$\frac{V_w}{V_p} = \frac{l_t - l_0}{l_0}, \tag{8a}$$

where l_0 and l_t correspond to the original and final sample lengths, respectively. In the case of MRI concentration profiles the calculation is expressed as:

$$\frac{V_w}{V_p} = \frac{1}{l_t}\int_0^{l_t} \phi_w dx, \tag{8b}$$

and for gravimetric data the swelling ratio is given as:

$$\frac{V_w}{V_p} = \frac{m_w}{m_p}\frac{\rho_p}{\rho_w}, \tag{8c}$$

where m_p is the mass of dry polymer, m_w is the mass of the water in the fully swollen polymer, and ρ_w and ρ_p are the densities of the water (1000 kg m^{-3}) and PEO (1200 kg m^{-3}), respectively.

The swelling kinetics for a sample are plotted in *Figure 11*. The kinetics follow the same trends against $t^{1/2}$ as the sample length kinetics reported in *Figure 9*, with the data showing a point of inflection. The length- and concentration-derived swelling ratios (*Figure 11*) obtained from MRI data are in very close agreement, which indicates that the concentration data are quantitatively accurate. Also, the gravimetric data are in close agreement with the length measurements, again reinforcing the finding that there is no significant volume change on mixing. The data presented are consistent with the swelling of crosslinked PEO in water, at room temperature, being a diffusion-controlled process.

CONCLUSIONS

A constrained swelling experiment has been developed in which one-dimensional swelling of the polymer sample is imposed by a glass tube. Used in conjunction with a one-dimensional, slice-selective, T_1-weighted MRI technique, this allows the rapid imaging of a high-swelling hydrogel *in situ*. Even though the n.m.r. spectra of the penetrant and polymer overlap, quantitative concentration profiles of both species can be measured in two ways. First, by using deuterated penetrant — the high mobility of the gelled polymer allows contrast-free ^1H images of the polymer distribution to be measured. Water profiles can be calculated by difference. Second, by using protonated penetrant and a two-component T_1-weighting technique to resolve the two

species from a simultaneous measurement, based on their different spin–lattice relaxation behaviour. The agreement between the profiles measured using the two techniques was excellent. It was found that there was no significant change in volume on mixing. The propagation of the front was found to be diffusion controlled. Further, it was possible to measure both the kinetics of the change in gel thickness as a function of penetration time and the swelling kinetics; the swelling of crosslinked PEO in water, at room temperature, was found to be a diffusion-controlled process.

The T_1 of the water in the gel was found to vary almost linearly with water concentration, whereas the T_1 of the polymer in the gel was relatively constant, suggesting that the mobility of the polymer chain segments is relatively constant once the polymer is in contact with water, regardless of concentration.

ACKNOWLEDGEMENTS

T. M. Hyde is grateful to the Association of Commonwealth Universities for the award of a Commonwealth Scholarship. The authors wish to thank the Process Engineering Committee of EPSRC for the award of the n.m.r. spectrometer. We also thank Dr M. R. Mackley for supplying us with PEO, and also for useful discussions.

REFERENCES

1. Mashelkar, R. A., *J. Indian Inst. Sci.*, 1993, **73**, 193.
2. Caruana, C. M., *Chem. Eng. Prog.*, 1992 (December), 12.
3. Hariharan, D. and Peppas, N. A., *J. Controlled Release*, 1993, **23**, 123.
4. Cook, R. L., King, H. E. and Peiffer, D. G., *Phys. Rev. Lett.*, 1992, **69**, 3072.
5. Graham, N. B., *Chemistry and Industry*, 1990 (6 August), 482.
6. Cima, L. G., *J. Cell. Biol.*, 1994, **56**, 155.
7. Schneider, N. S., Illinger, J. L. and Karasz, F. E., *J. Appl. Polym. Sci.*, 1993, **48**, 1723.
8. Embrey, M. P., Graham, N. B., McNeill, M. E. and Hillier, K., *J. Controlled Release*, 1986, **3**, 39.
9. Long, F. A. and Richman, D., *J. Am. Chem. Soc.*, 1960, **82**, 513.
10. Thomas, N. L. and Windle, A. H., *Polymer*, 1977, **18**, 1195.
11. Gyor, M., Rockenbauer, A., Jokay, L. and Tudos, F., *Polym. Bull.*, 1986, **15**, 525.
12. Mills, P. J., Palmstrøm, C. J. and Kramer, E. J., *J. Mater. Sci.*, 1986, **21**, 1479.
13. Fieldson, G. T. and Barbari, T. A., *Polymer*, 1993, **34**, 1146.
14. Blümich, B. and Blümer, P., *Makromol. Chem.*, 1993, **194**, 2133.
15. Weisenberger, L. A. and Koenig, J. L., *Appl. Spectrosc.*, 1989, **43**, 1117.
16. Weisenberger, L. A. and Koenig, J. L., *J. Polym. Sci., Polym. Lett. Ed.*, 1989, **27**, 55.
17. Weisenberger, L. A. and Koenig, J. L., *Macromol.*, 1990, **23**, 2445.
18. Weisenberger, L. A. and Koenig, J. L., *Macromol.*, 1990, **23**, 2454.
19. Tabak, F. and Corti, M., *J. Chem. Phys.*, 1990, **92**, 2673.
20. Ilg, M., Pfleiderer, B., Albert, K., Rapp, W. and Bayer, E., *Macromol.*, 1994, **27**, 2778.
21. Blackband, S. and Mansfield, P., *J. Phys. C*, 1986, **19**, L49.
22. Mansfield, P., Bowtell, R. and Blackband, S., *J. Magn. Reson.*, 1992, **99**, 507.
23. Fyfe, C. A., Randall, L. H. and Burlinson, N. E, *J. Poly. Sci.: Part A: Polym. Chem.*, 1993, **31**, 159.
24. Webb, A. G. and Hall, L. D., *Polym. Commun.*, 1990, **31**, 422.
25. Webb, A. G. and Hall, L. D., *Polym. Commun.*, 1990, **31**, 425.
26. Webb, A. G. and Hall, L. D., *Polymer*, 1991, **32**, 2926.
27. Hyde, T. M., Gladden, L. F., Mackley, M. R. and Gao, P., *J. Polym. Sci., Polym. Chem. Ed.*, 1995, **33**, 1795.
28. Köller, G., Köller, E., Kuhn, W. and Moll, F., *Pharm. Ind.*, 1991, **53**, 955.
29. Rajabi-Siahboomi, A. R., Bowtell, R. W., Mansfield, P., Henderson, A., Davies, M. C. and Melia, C.D., *J. Controlled Release*, 1994, **31**, 121.
30. Hyde, T. M., Gladden, L. F. and Payne, R., *J. Controlled Release*, 1995, **36**, 261.
31. Halse, M. R., Rahman, H. J. and Strange, J. H., *Physica B*, 1994, **203**, 169.
32. Graham, N. B. and McNeill, M. E., *Makromol. Chem. Macromol. Symp.*, 1988, **19**, 255.
33. Fukushima, E. and Roeder, S. B. W., *Experimental Pulse NMR: A Nuts and Bolts Approach*. Addison-Wesley, New York, 1981.
34. Cheng, H. N. and Early, T. A., *Macromol. Symp.*, 1994, **86**, 1.
35. Edelstein, W. A., Hutchinson, J. M. S., Johnson, G. and Redpath, T. W., *Phys. Med. Biol.*, 1980, **25**, 751.
36. Callaghan, P. T., *Principles of Nuclear Magnetic Resonance Microscopy*. Oxford University Press, Oxford, 1991.
37. Garroway, A. N., Grannell, P. K. and Mansfield, P., *J. Phys. C*, 1974, **7**, L457.
38. Buszko, M. and Maciel, G. E., *J. Magn. Reson. A*, 1994, **107**, 151.
39. Alfrey, T., Gurnee, E. F. and Lloyd, W. G., *J. Polym. Sci.*, 1966, **C12**, 249.
40. Thomas, N. L. and Windle, A. H., *Polymer*, 1982, **23**, 529.
41. Park, G. S. and Crank, J., *Diffusion in Polymers*. Academic Press, New York, 1968.